2008 International Symposium on Nonlinear Theory and its Applications
NOLTA'08, Budapest, Hungary, September 7-10, 2008

A transfer operator based numerical investigation of coherent structures in three-dimensional Southern ocean circulation

Gary Froyland†, Marcel Schwalb‡, Kathrin Padberg⋆ and Michael Dellnitz‡

†School of Mathematics and Statistics, University of New South Wales, Sydney NSW 2052, Australia
‡Department of Mathematics, University of Paderborn, D-33095 Paderborn, Germany
⋆ Institute for Transport and Economics, Dresden University of Technology, D-01062 Dresden, Germany
Email: g.froyland@unsw.edu.au, schwalb@math.upb.de, padberg@vwi.tu-dresden.de, dellnitz@upb.de

Abstract—We report on a numerical investigation of three-dimensional circulation in the Southern Ocean over a domain extending from Antarctica to -36 degrees latitude and from the sea surface to a depth of 500 metres. The high latitude Southern Ocean is a region low in measurements but important for climatic and biological applications. Our investigation is based upon velocity data simulated by a state-of-the-art 1/4 degree resolution global ocean model. We construct an approximate transfer operator from the velocity data and identify dominant coherent circulation structures from eigenmodes of the transfer operator.

1. Introduction

Coherent structures play a crucial role in explaining transport in non-autonomous dynamical systems such as ocean flows. Their ecological impact includes the trapping of material such as nutrients, phytoplankton, and pollutants. These Lagrangian structures are very difficult to identify as they are not revealed by the underlying Eulerian velocity fields.

While persistent ocean features such as gyres and eddies may be observed and tracked by satellite altimetry [1], detecting and tracking the regions that act as barriers to Lagrangian flow pathways is more ambiguous. This is true even if the velocity field is perfectly known.

Froyland *et al.* [2] applied transfer operator techniques to identify two key coherent structures in the Southern Ocean, namely the Weddell and Ross Gyres. The transfer operator approach identified gyre regions on the ocean surface with 10% greater coherence than standard oceanographic techniques based on sea surface height measurements. The less direct method of finite time Lyapunov exponents was also studied in [2] and was found to perform extremely poorly.

The study [2] was restricted to surface ocean flow. In the present work we extend the techniques used in [2] to the full three-dimensional flow. Our method is based upon numerically constructing a transfer operator that controls the ocean circulation from a time t to a short time later $t+\tau$. The eigenfunctions of this transfer operator corresponding to large positive eigenvalues directly reveal dominant "almost-invariant" structures in the surface flow over the time period considered. These structures retain their shape over the period $[t, t+\tau]$ and thus "trap" most of the water inside them with only minimal leakage. In addition, our approach allows us to quantify the mass leakage of the identified regions. We demonstrate that the surface gyre features reported in [2] in fact extend deep below the surface to control particle transport over large regions of the Southern Ocean.

2. Input data and non-autonomous flow model

Our input data is generated by the ORCA025 global ocean model [3]. In the Southern Ocean, the model grid follows a Mercator projection. Eddy characteristics of the model compare favorably with satellite and drifter observations [3]. In this paper we use the data of the year 2004. The available model output consists of 3D fields of velocity averaged over a month.

As we consider the Southern Ocean we work on a subset X of a solid annulus $\mathfrak{X} = S^1 \times [-76, -36] \times [-500, 0)$ with S^1 parameterised in degrees from -180^o to 180^o. Considered as a non-autonomous dynamical system, the ocean flow may be described by $(x, t, \tau) \mapsto \Phi(x, t; \tau)$, where $\Phi : X \times \mathbb{R} \times \mathbb{R} \to X$ and $\Phi(x, t; \tau)$ is the terminal point in X of a trajectory beginning at $x \in X$ at time t and flowing for τ time units. A trajectory $x(t) := \Phi(x_0, t_0; t)$ is a solution to the non-autonomous ODE $\frac{dx}{dt} = f(x(t), t)$ with initial condition $x(t_0) = \Phi(x_0, t_0; 0)$. The vector field $f : X \times \mathbb{R} \to \mathbb{R}^3$ is obtained from the output of the ORCA025 model. We note that the ocean flow is volume preserving.

2.1. Vertical transport associated with the mixed layer

Vertical transport of particles is modelled in two ways. Vertical transport associated with subduction is already included as vertical particle velocities in the ORCA025 vector field. These vertical velocities accurately represent vertical particle transport in the deep ocean, however, nearer to the ocean surface the mixing of particles due to wind-driven currents and the breaking of surface waves is very high. The *mixed layer* (ML) refers to a layer near the surface where this more rapid mixing occurs. This layer extends from the surface down to the *mixed layer depth*

(MLD). The ORCA025 model provides a monthly integrated MLD field which is based on the difference between the density at the surface and the density at depth. The depth at which this difference exceeds $0.3\text{kg} \cdot \text{m}^{-3}$ is the mixed layer depth; see [4]. Within the ML, temperature and salinity are almost constant. The depth of the ML varies from day to day and from season to season. Due to surface cooling and the resulting gravitational instability, mixed layers are generally deeper during late winter and shallowest during summer.

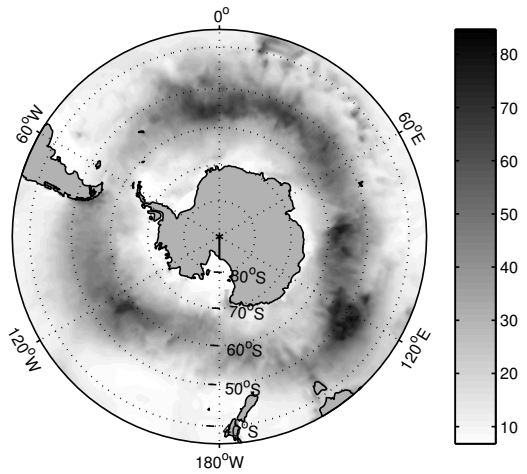

Figure 1: The mixed layer depth in metres on X during January 2004.

3. Almost-invariant sets, coherent structures, and transfer operators

Let μ denote three dimensional volume measure, normalised so that $\mu(X) = 1$. The measure μ is invariant under Φ; formally, for each $\tau \geq 0$, $\mu(\Phi(A, t; -\tau)) \approx \mu(A)$. We will say that a set $A \subset X$ is $\Phi-$*invariant* over $[t, t+\tau]$ if $A = \Phi(A, t+s; -s))$ for all $0 \leq s \leq \tau$. Coherent structures obey an approximate invariance principle over short periods of time. We shall call a set $A \subset X$ *almost-invariant* if

$$\rho_{t,\tau}(A) := \frac{\mu(A \cap \Phi(A, t+\tau; -\tau))}{\mu(A)} \approx 1. \qquad (1)$$

The ratio in (1) is the proportion of the set A that remains in A under the flow from time t to time $t+\tau$. Clearly, the closer this ratio is to unity, the closer the set A is to being invariant. In order to discover coherent structures in the flow Φ, we seek to find dominant almost-invariant sets.

The notion of almost-invariant sets arose as a means of discovering dominant geometric structures in general dynamical systems [5] and has been refined and applied in a variety of settings, e.g. [6, 7, 8]. In order to locate these almost-invariant sets we introduce a transfer operator describing flows for short periods.

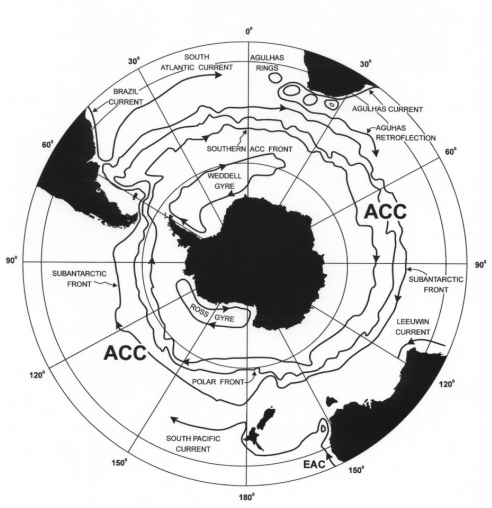

Figure 2: Coherent structures for the Southern Ocean, including the Antarctic Circumpolar Current and its three associated fronts, the Weddell Gyre, and the Ross Gyre.

We define a linear operator $\mathcal{P}_{t,\tau} : L^1(X, m) \circlearrowleft$ by

$$\mathcal{P}_{t,\tau} g(x) = \frac{g(\Phi(x, t+\tau; -\tau))}{|\det D\Phi(\Phi(x, t+\tau; -\tau), t; \tau)|}. \qquad (2)$$

If there is a Φ-invariant set $A \subset X$ over $[t, t+\tau]$, then $\mathcal{P}_{t,\tau}\chi_A = \chi_A$. Thus χ_A is an eigenfunction of $\mathcal{P}_{t,\tau}$ with eigenvalue 1. Sets A that are *almost-invariant correspond to eigenfunctions of* $\mathcal{P}_{t,\tau}$ *with real eigenvalues very close to 1* [5, 7].

To access these eigenfunctions numerically, we construct a finite-dimensional Galerkin approximation of $\mathcal{P}_{t,\tau}$ based on a fine partition $\{B_1, \ldots, B_n\}$ of X. Following Ulam's approach [5, 6, 7, 8] we form the transition matrix

$$\mathbf{P}_{t,\tau;i,j} = \frac{m(B_i \cap \Phi(B_j, t+\tau; -\tau))}{m(B_i)}. \qquad (3)$$

The matrix $\mathbf{P}_{t,\tau}$ is stochastic. The entry $\mathbf{P}_{t,\tau;i,j}$ may be interpreted as the probability that a point selected uniformly at random in B_i at time t will be in B_j at time $t+\tau$.

4. Numerical implementation

4.1. Oceanic domain and discretization

For our computational studies we create a partition of $\mathfrak{X}$ via a uniform three-dimensional grid of $m = 114688$ boxes. Each box has side lengths of 1.4 degrees longitude, 1.4 degrees latitude, and 31.25 metres depth. We set $X = \bigcup_{i:\|f(x,t_0)\|>10^{-6} \ \forall \ x \in B_i} B_i$, where t_0 denotes January 1st 2004. X is an approximation of the oceanic domain with the continents and islands removed where $n = 92518$.

To calculate the transition matrix $\mathbf{P}_{t,\tau}$, each box B_i, $i = 1, \ldots, n$ is filled with N uniformly distributed test points

$y_{i,\ell} \in B_i$, $\ell = 1, \ldots, N$. For each $i = 1, \ldots, n$ we calculate $\Phi(y_{i,\ell}, t; \tau)$, $\ell = 1, \ldots, N$ by numerical integration and set

$$\mathbf{P}_{t,\tau;i,j} \approx \frac{\#\{\ell : y_{i,\ell} \in B_i, \Phi(y_{i,\ell}, t; \tau) \in B_j\}}{N} \tag{4}$$

where $N = 512$ in the experiments reported here. The box-discretization of $\mathfrak{X}$ and the construction of $\mathbf{P}_{t,\tau}$ is carried out efficiently using the software package GAIO [9].

4.2. Model interpolation and trajectory integration

The ORCA025 model is given at a resolution of 0.25 degrees of longitude and latitude, and 46 non-uniform depth layers. Velocity field values for x lying between grid points are affinely interpolated independently in the longitude, latitude and depth directions. The velocity field $f(x, t)$ for t between grid points is produced by linear interpolation. Calculation of $\Phi(y_{i,\ell}, t; \tau)$ is carried out using a standard Runge-Kutta approach with stepsize of 3 days. Within 3 days the vast bulk of trajectories will flow only to a neighbouring grid set in the grid upon which the velocity field is defined. Since $f(x, t)$ is independently affine between grid points, the numerical integration error should be small. We refer the reader to [2] for a discussion on choice of box discretisation versus flow time τ.

4.3. Computation of MLD mixing

The mixed layer particle mixing is not captured by the vector field f. We make a standard assumption that the ML is well mixed. In order to simulate this with our sample trajectories, we proceed as follows. We write $y \in X$ as $y = (\mathrm{Lon}(y), \mathrm{Lat}(y), \mathrm{Dep}(y))$, and let $\mathrm{MLD}(t, \mathrm{Lon}(y), \mathrm{Lat}(y))$ denote the mixed layer depth for the water column located at $(\mathrm{Lon}(y), \mathrm{Lat}(y))$ at time t.

1. Integrate test point $y_{i,\ell}$ for one month ($\tau = 1$) to produce $y' := \Phi(y_{i,\ell}, t_0; 1)$.
2. Test whether y' lies in the ML for the current month. If it does, replace y' with $(\mathrm{Lon}(y'), \mathrm{Lat}(y'), z_{\mathrm{pert}})$ where z_{pert} is randomly sampled from a uniform distribution on the interval $[\mathrm{MLD}(t, \mathrm{Lon}(y'), \mathrm{Lat}(y')), 0]$. If y' does not lie in the ML, make no vertical perturbation.
3. Integrate y' for a further month and repeat step 2.

4.4. Eigenvalue and eigenfunction calculation

Define a probability measure μ_n on $X = \bigcup_{i=1}^n B_i$ by

$$p_i = \frac{\text{Volume of } B_i}{\text{Volume of } X}, \tag{5}$$

and $\mu_n(A) = \sum_{i=1}^n p_i \cdot m(A \cap B_i)/m(B_i)$. Let $A = \bigcup_{i \in \mathcal{I}} B_i$ where $\mathcal{I} \subset \{1, \ldots, n\}$. Then it is straightforward to show [7]

$$\rho_{t,\tau}(A) \approx \frac{\sum_{i,j \in \mathcal{I}} p_i \mathbf{P}_{t,\tau;i,j}}{\sum_{i \in \mathcal{I}} p_i}. \tag{6}$$

The expression (6) is very close to equality and in the limit as $n \to \infty$ and the diameter of the boxes $\{B_i\}_{i=1}^n$ approaches zero, one obtains equality.

We transform the matrix $\mathbf{P}_{t,\tau}$ into a "time symmetric" matrix $R_{t,\tau}$ via

$$R_{t,\tau;i,j} = \left(\mathbf{P}_{t,\tau;i,j} + \frac{p_j \mathbf{P}_{t,\tau,j,i}}{p_i} \right) / 2. \tag{7}$$

The matrix R is stochastic, has p as a fixed left eigenvector, and satisfies important maximization properties [8] related to almost-invariance. As in [8] we use the right eigenvectors $v^{(k)}$ of R to detect almost-invariant sets. The matrix $R_{t,\tau;i,j}$ is typically very sparse and we are interested only in the large spectral values near to 1, which may be efficiently computed by Lanczos iteration methods.

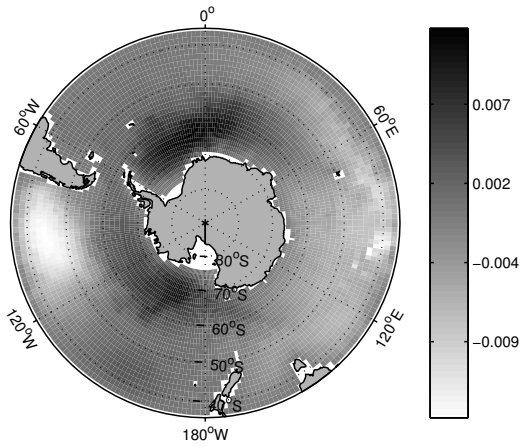

Figure 3: Coherent structures in the Weddell and Ross Seas are highlighted by large values of $w := v^{(4)} + v^{(6)}$.

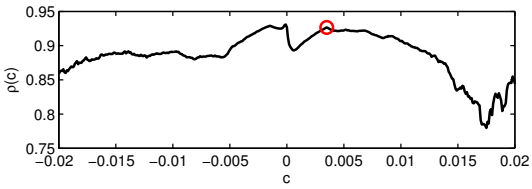

Figure 4: Values of $\min\{\rho(A_c^+), \rho(A_c^-)\}$ vs. c. We choose the global maximum for positive c as we wish to select dark coloured regions. See [10] for further details on the method of selecting c.

5. Results

We demonstrate that our method detects persistent structures in the Southern Ocean flow in the Weddell and Ross Seas. We computed the 20 largest eigenvalues of R (ranging from $\lambda_2 = 0.9933$ to $\lambda_{20} = 0.9796$) and the corresponding right eigenvectors. The fourth eigenfunction

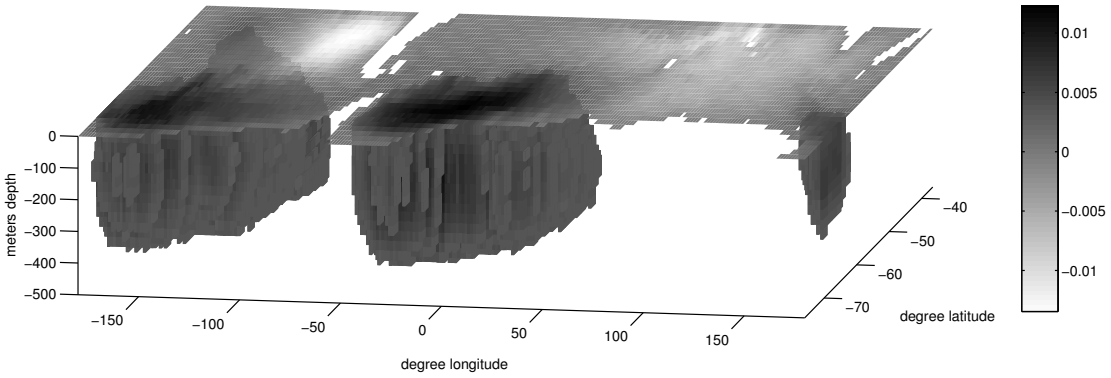

Figure 5: Three-dimensional coherent structures in the Weddell and Ross Seas, and in the South Pacific are highlighted by large values of w. Boxes B_i, $i = 1, \ldots, n$ with $w_i < c = 0.0035$ have been removed.

(corresponding to $\lambda_4 = 0.9910$) identifies a coherent structure in the Weddell Sea, and the sixth eigenfunction identifies a coherent structure in the Ross Sea (corresponding to $\lambda_6 = 0.9884$). Both structures are visible on the ocean surface. In order to treat both structures simultaneously we consider a linear combination of the two eigenfunctions $w := v^{(4)} + v^{(6)}$, see Figure 3 for w restricted to the surface. These results are in very good agreement to the studies in [2] where only the surface velocity field was considered and not the full 3d dynamics as here. They also closely match the gyres shown in Figure 2.

To extract the coherent structures we use a heuristic ansatz as described in [10] (see also [7]): we define sets A_c^+ and A_c^- by

$$A_c^+ := \bigcup_{i:w_i \geq c} B_i, \qquad A_c^- := \bigcup_{i:w_i < c} B_i, \tag{8}$$

and choose c in such that a way that both $\rho(A_c^-)$ and $\rho(A_c^+)$ are maximized, see Figure 4. The application of this approach gives three subsurface structures as A_c^+ (where $c = 0.0035$), two in the Weddell and Ross Seas respectively, and another in the Southern Pacific Ocean, see Figure 5. We obtain a coherence value of $\rho(A_c^+) = 0.9266$, or in other words, 92.7% of water mass is retained in A_c^+ after two months of flow. If we consider the coherence of the two gyres without the Southern Pacific Ocean structure, we obtain $\rho(A_c^{+,W}) = 0.9293$, or 92.9% of the water mass is retained in the Weddell region, and $\rho(A_c^{+,R}) = 0.8972$ for the Ross region.

Acknowledgements

The authors thank Matthew England for very helpful discussions on MLD and Agus Santoso for assistance with computing the MLD.

References

[1] L.-L. Fu. Pathways of eddies in the South Atlantic Ocean revealed from satellite altimeter observations. *Geophysical Research Letters*, 33:L14610, 2006.

[2] G. Froyland, K. Padberg, M. England, and A.M. Treguier. Detection of Coherent Oceanic Structures via Transfer Operators. *Physical Review Letters*, 98(22):224503, 2007.

[3] B. Barnier *et al.* Impact of partial steps and momentum advection schemes in a global ocean circulation model at eddy permitting resolution. *Ocean Dynamics*, 56(5-6):543–567, 2006.

[4] S.M. Griffies *et al.* Coordinated ocean-ice reference experiments. Submitted, 2008.

[5] M. Dellnitz and O. Junge. On the approximation of complicated dynamical behavior. *SIAM Journal on Numerical Analysis*, 36(2):491–515, 1999.

[6] M. Dellnitz *et al.* Transport in dynamical astronomy and multibody problems. *International Journal of Bifurcation and Chaos*, 15(3):699–727, 2005.

[7] G. Froyland and M. Dellnitz. Detecting and locating near-optimal almost-invariant sets and cycles. *SIAM Journal on Scientific Computing*, 24(6):1839–1863, 2003.

[8] G. Froyland. Statistically optimal almost-invariant sets. *Physica D*, 200:205–219, 2005.

[9] M. Dellnitz, G. Froyland, and O. Junge. The algorithms behind GAIO – Set oriented numerical methods for dynamical systems. In B. Fiedler, editor, *Ergodic Theory, Analysis, and Efficient Simulation of Dynamical Systems*, pages 145–174. Springer, 2001.

[10] G. Froyland and K. Padberg. Almost-invariant sets and invariant manifolds – connecting probabilistic and geometric descriptions of coherent structures in flows. Submitted, 2008.